Computational and experimental investigation of intermolecular states and forces in the benzene–helium van der Waals complex

Soohyun Lee, James S. Chung, and Peter M. Felker[a]
Department of Chemistry and Biochemistry, University of California, Los Angeles, California 90095-1569

Javier López Cacheiro and Berta Fernández
Department of Physical Chemistry, Faculty of Chemistry, University of Santiago de Compostela, E-15782 Santiago de Compostela, Spain

Thomas Bondo Pedersen
Institute of Molecular Science, University of Valencia, E-46100 Burjassot, Valencia, Spain

Henrik Koch
Department of Chemistry, Norwegian University of Science and Technology N-7491 Trondheim, Norway

A study of the intermolecular potential-energy surface (IPS) and the intermolecular states of the perprotonated and perdeuterated benzene–He complex is reported. From a fit to *ab initio* data computed within the coupled cluster singles and doubles including connected triples model for 280 interaction geometries, an analytic IPS including two- to four-body atom–atom terms is obtained. This IPS, and two other Lennard-Jones atom–atom surfaces from the literature, are each employed in dynamically exact (within the rigid-monomer approximation) calculations of $J=0$ intermolecular states of the isotopomers. Rotational constants and Raman-scattering coefficients for intermolecular vibrational transitions are also calculated for each of the three surfaces. The calculated results are compared with experimental results reported herein pertaining to intermolecular Raman spectra of benzene–He. The calculated rotational constants are compared with experimental values from the literature. The fitted IPS of this work leads to calculated observables that match the experimental results very well. The IPSs from the literature are not as successful, specifically in regard to the intermolecular Raman spectra. © *2003 American Institute of Physics.* [DOI: 10.1063/1.1628217]

I. INTRODUCTION

Helium-containing van der Waals molecules were among the first weakly bound species to be studied by laser spectroscopy of cold molecular-beam samples.[1–6] Interest in such species has continued into the present[7–21] for several reasons. First, the intermolecular forces pertaining to them are relatively simple. Thus, one has the expectation that quantitative comparison between results from *ab initio* calculations of cluster properties and those from experiment should be feasible for such species (e.g., see Ref. 18 and references therein). Second, the small intermolecular bond energies of molecule–He complexes, together with the small complexation-induced perturbation of the intramolecular level structure of the molecular moiety, render the species particularly useful as model systems for the investigation of predissociation and intramolecular vibrational energy-flow dynamics (e.g., Refs. 4, 13, 15). Third, the complexes can exhibit very large-amplitude intermolecular motions at low, readily accessible excitation energies (e.g., see Refs. 17, 21). Hence, they are good species for the investigation and modeling of such motions. Finally, relatively recent developments have made possible the study of molecule-doped helium droplets.[22] The promise that such experiments have in

regard to the molecular spectroscopy of nonvolatile and transient species and the characterization of fluid dynamics on a nanoscopic scale highlights the need for a fuller characterization of the forces between helium atoms and polyatomics—the kind of information that is available, in principle, from studies of molecule–He complexes.

One class of molecule–He complexes that has been the subject of numerous studies, experimental and computational, is that for which the molecule is an aromatic species. Among such studies are ones involving helium complexes of *s*-tetrazine,[3,7,9] benzene,[5] aniline,[10,12,16] *t*-stilbene,[8,11,13,15] *p*-methyl-*trans*-stilbene,[14] 1,2-dimethylnaphthalene,[17] and naphthalene, anthracene, and tetracene.[19,20] In addition, work pertaining to larger clusters involving an aromatic molecule solvated by several[19–21] or many helium atoms[23,24] has also been reported. One of the interests in these species lies in the fact that they represent useful systems for gaining insight into the behavior of helium on graphite surfaces. Further, the anisotropy of the aromatic–He interaction leads to interesting large-amplitude motions of the helium atoms, even at very low excitation energies. Finally, the ability to systematically vary the aromatic–He interaction by changing the characteristics of the aromatic moiety provides a means by which to probe systematically the influences of solute on the unique properties of liquid helium.[24]

[a]Electronic mail: felker@chem.ucla.edu

12956

Despite the considerable interest in aromatic–He_n complexes and clusters, quantitative information pertaining to aromatic–He intermolecular potential-energy surfaces (IPSs) and the testing of such surfaces against experimental results is rather limited. Our aim in this paper is to further the progress in this area by reporting on a computational and experimental investigation of the IPS governing the interaction between helium and benzene. In particular, we have performed coupled-cluster singles and doubles with connected triples[25] [CCSD(T)] *ab initio* electronic-structure calculations of benzene–He interaction energies over a wide range of geometries. We have also fitted these interaction energies to an analytic function to obtain a fitted IPS accurate to 0.5 cm^{-1} (root-mean-squared) with respect to the *ab initio* results. Second, we have performed dynamically exact (within the rigid-monomer approximation) calculations of the $J=0$ intermolecular states of the benzene–He van der Waals complex for this fitted IPS, as well as for two other IPSs that have appeared in the literature. From these results we have also computed rotational constants and matrix elements relevant to spectroscopic transitions between the intermolecular states. Finally, we have performed experiments involving the measurement of intermolecular Raman spectra for the perprotonated and perdeuterated benzene–He species. Besides adding to the rather sparse body of experimental results relating to intermolecular level structures of He-containing complexes, comparison of these results on benzene–He with the results of our intermolecular-state calculations provides a test of the accuracy of the IPSs employed in the latter. In this comparison the fitted IPS presented here holds up well. The other two IPSs are found to be lacking. The implications of these results are discussed.

The paper is organized as follows: Section II pertains to the electronic structure calculations and the fitting of the results of those calculations to obtain an analytic IPS. The characteristics of the IPS are also considered. Section III deals with the methods and results relating to the numerical solution of the intermolecular Schrödinger equation for the benzene–He complex. Section IV outlines the procedures employed to measure intermolecular Raman spectra of the perprotonated and perdeuterated benzene–He complexes. In Sec. V the experimental results are presented. Section VI is a concluding discussion.

II. COMPUTED INTERMOLECULAR POTENTIAL-ENERGY SURFACE

A. *Ab initio* calculations

Benzene–He interaction energies were calculated by *ab initio* electronic-structure techniques for 309 interaction geometries. The calculations were performed at a level found to yield excellent agreement with experiment for other benzene-containing van der Waals complexes.[26–29] That is, the coupled cluster singles and doubles including connected triples corrections [CCSD(T)] model[25] with an augmented correlation-consistent polarized-valence atomic basis set (aug-cc-pVDZ) extended with a set of

$3s3p2d1f1g$ (33 211) bond functions (see, e.g., Ref. 26 for the exponents defining the 33 211 set) was employed. The bond functions were placed in the middle of the vector joining the benzene center of mass with the He nucleus. The benzene moiety was taken to have a fixed D_{6h} planar geometry with $R_{CC}=1.397$ Å and $R_{CH}=1.08$ Å. The position of the He nucleus relative to the benzene center of mass varied over a volume encompassing distances from 0 to 5 Å above the ring plane and 0 to 7 Å from the benzene C_6 axis. All interaction energies were counterpoise corrected[30] and were computed in the frozen-core approximation by the DALTON program.[31–33] The complete set of geometries and interaction energies is available from Ref. 34.

B. Fitted potential surface

The *ab initio* results corresponding to interaction energies less than the benzene–He dissociation energy (280 data points) were fitted (Marquardt's nonlinear least-squares algorithm[35]) to an analytic function, $V_{fit}(\mathbf{d})$, containing 18 adjustable parameters. The functional form used is very similar to that employed by some of us[28] in the fitting of IPS data on a similar species (i.e., benzene–Ar). It is given by

$$V_{fit}(\mathbf{d})=C_0+W_0\left[\sum_k V_2(r_k)+\sum_{l<k} V_3(r_k,r_l)\right.$$
$$\left.+\sum_{m<l<k} V_4(r_k,r_l,r_m)\right]. \quad (1)$$

Here, $\mathbf{d}$ is the position vector from the benzene center of mass to the He nucleus, with its components (x,y,z) measured with respect to a Cartesian coordinate system defined by an $\hat{x}$ axis parallel to a C–C bond bisector, a $\hat{y}$ axis parallel to a C–H bond, and a $\hat{z}$ axis parallel to the benzene C_6 symmetry axis and completing a right-handed coordinate system. Further

$$r_k\equiv[(x-X_k)^2+(y-Y_k)^2+b_z(z-Z_k)^2]^{1/2} \quad (2)$$

is a modified distance between the He and the kth carbon nucleus located at (X_k,Y_k,Z_k),

$$V_2(r_k)\equiv w^2(r_k)+\sum_{i=3}^5 c_i w^i(r_k)+c_6\widetilde{w}^6(r_k) \quad (3)$$

contains two-body terms,

$$V_3(r_k,r_l)\equiv\sum_{i=1}^2 c_{ii}w^i(r_k)w^i(r_l)+\sum_{i<j} c_{ij}[w^i(r_k)w^j(r_l)$$
$$+w^i(r_l)w^j(r_k)] \quad (4)$$

contains three-body terms,

$$V_4(r_k, r_l, r_m) \equiv c_{111} w(r_k) w(r_l) w(r_m) + c_{122}[w(r_k)w^2(r_l)w^2(r_m) + w^2(r_k)w^2(r_l)w(r_m) + w^2(r_k)w(r_l)w^2(r_m)]$$

$$+ \sum_{i=2}^{3} c_{11i}[w(r_k)w(r_l)w^i(r_m) + w(r_k)w^i(r_l)w(r_m) + w^i(r_k)w(r_l)w(r_m)] \qquad (5)$$

contains four-body terms,

$$w(r_k) \equiv 1 - \exp[-a(r_k - r_0)], \qquad (6)$$

$\tilde{w}(r_k) = w(r_k)$ if $r_k \geq r_0$ and $\tilde{w}(r_k) = 0$ if $r_k < r_0$, and

$$C_0 \equiv 6[1 + c_3 + c_4 + c_5 + c_6] + 15[c_{11} + c_{22} + 2(c_{12} + c_{13} + c_{14} + c_{23})] + 20[c_{111} + 3(c_{112} + c_{113} + c_{122})]. \qquad (7)$$

$[C_0$ ensures $V_{\text{fit}}(\mathbf{d}) \to 0$ for $|\mathbf{d}| \to \infty$.] The 18 fitting parameters in $V_{\text{fit}}(\mathbf{d})$ are listed in Table I. The parameters produce a standard deviation of 0.5 cm^{-1} between the fitted IPS (which we henceforth shall label "IPS-A") and the *ab initio* points. The deviations of IPS-A from the *ab initio* energies at each of the grid points used in the fit are reported in Ref. 34.

Figure 1 shows contour plots relating to four cuts of IPS-A. The first lines of Table II summarize information relating to the fixed points on the surface. The overall shape of the surface is similar to surfaces computed by similar means for the S_0 and S_1 electronic states of benzene–Ar.[28] That is, there are two global minima corresponding to central binding of the He along the C_6 axis of benzene. There are six equivalent local minima in the benzene plane at the periphery of the ring along bisectors of the C–C bonds. There are six equivalent saddle points, located in the benzene plane along C–H bond vectors, that separate these local minima. And, there are six equivalent saddle points on each side of the benzene plane that lie along the minimum-energy paths from global minimum #1-to-in-plane local minimum-to-global minimum #2. Given the light mass of He and by analogy to the cyclopropane–He complex,[36] the relative energies of these fixed points are such that one might expect appreciable splittings due to ring–plane crossings of the atom in the

benzene–He complex. This expectation is borne out by the results of calculations of intermolecular states, as reported below.

III. CALCULATION OF INTERMOLECULAR STATES AND TRANSITION INTENSITIES

A. Intermolecular potential-energy surfaces

Direct tests of the accuracy of an IPS require the comparison of experimental observables with calculations of those observables under the assumption that the IPS in question governs the intermolecular interaction. We have performed calculations of intermolecular level structure, intermolecular Raman-transition intensities, and rotational constants for benzene–He using IPS-A. In the interest of helping to assess the accuracy of other IPSs relating to benzene–He, we have also performed such calculations for two other surfaces. One of these ("IPS-B") was constructed from the generic aromatic–He, Lennard-Jones, atom–atom pair-potential parameters of Ref. 21. This approach toward obtaining an aromatic–He IPS from a transferable set of parameters has been employed in studies of several helium-containing complexes and clusters (e.g., see Refs. 15, 17, 21). Another potential ("IPS-C") was taken from Ref. 24, wherein it was employed in Feynmann path-integral calculations of benzene–He$_n$ cluster properties. This generalized (angle-dependent) Lennard-Jones, atom–atom pair-potential surface was obtained from a fit to the *ab initio* data of Ref. 37. For all three IPSs we took the C–C and C–H bond lengths to be 1.397 and 1.08 Å, respectively.

It is pertinent to examine briefly some of the features of IPS-B and IPS-C. The two surfaces differ significantly from one another and from IPS-A. Table II summarizes information related to the fixed points of these surfaces in addition to those of IPS-A. IPS-A and IPS-B appear somewhat similar to one another in respect to the positions and energies of their fixed points. However, the minima along the C–C bisectors for IPS-A are saddle points for IPS-B. Moreover, the saddle points above and below the benzene plane for IPS-A (at -28.87 cm^{-1}) have no counterparts for IPS-B. Most pertinent, though, x, y contour plots for $z = z_e$ (z_e being the z value at the global minimum) show that confinement in the x, y directions is considerably tighter for IPS-A than it is for IPS-B. In regard to IPS-C, three of its fixed-point types are of the same qualitative nature as those of IPS-B. It has considerably more structure than the latter surface, though, as evidenced by the presence of four additional fixed-point types. Further, and most important, IPS-C is shifted to significantly higher energies than either of the other two surfaces over most of the relevant three-dimensional space, and, like IPS-B, the x, y confinement near $z = z_e$ is less tight than for IPS-A.

TABLE I. Parameters of the analytic benzene–helium IPS (V_{fit} or IPS-A) fitted to the *ab initio* data. The value of the IPS is zero for infinite separation of the benzene and helium.

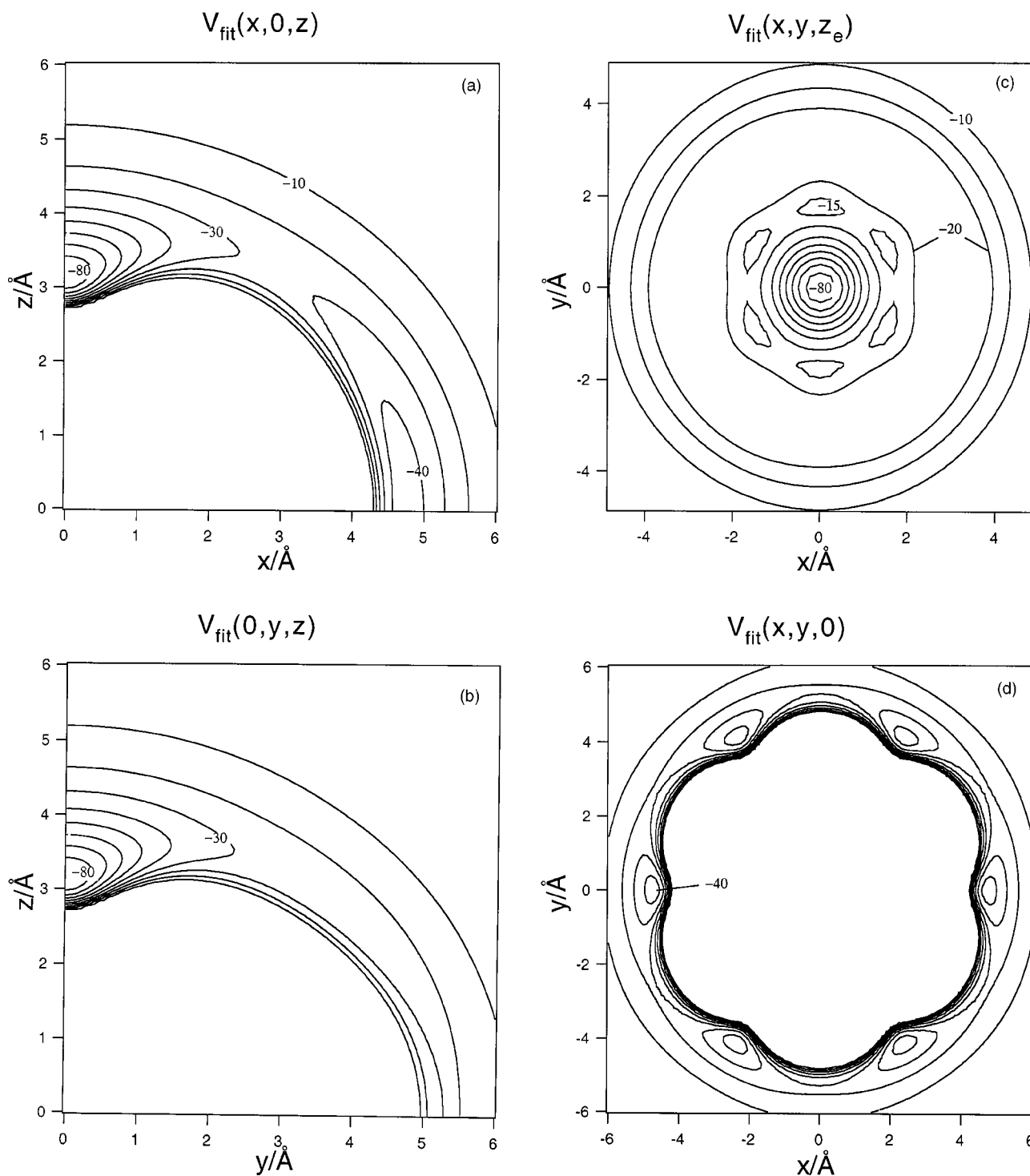|	
r_0 /Å	7.220 527
a/Å^{-1}	0.572 446
b_z	1.264 890
W_0 /cm^{-1}	0.023 767
c_3	0.058 387
c_4	$-6.914\ 851$
c_5	$-2.083\ 808$
c_6	85.429 568
c_{11}	$-16.956\ 997$
c_{12}	0.586 429
c_{22}	9.073 184
c_{13}	1.821 920
c_{14}	1.874 776
c_{23}	$-0.098\ 396$
c_{111}	$-3.235\ 122$
c_{112}	$-2.631\ 504$
c_{122}	1.423 777
c_{113}	$-2.117\ 152$

FIG. 1. Contour plots of V_{fit} (IPS-A). (a) The $y=0$ plane. (b) The $x=0$ plane. (c) The $z=3.157$ Å plane. (d) The $z=0$ plane. The energy figures are given in cm^{-1}. The contour lines are separated by 10 cm^{-1} except for the -15 cm^{-1} contours in (c).

B. $J=0$ Intermolecular level structure

In a previous work on benzene–Ar (Ref. 38) we have described an approach involving filter-diagonalization[39–41] variational calculations of intermolecular states in benzene–atom complexes. We use a similar approach here in application to benzene–He. The only procedural difference between the work reported here and the prior report arises from the

need to consider rare-gas-atom tunneling from one side of the benzene plane to the other in the He case, whereas no such consideration is needed in the Ar case.

Briefly, we express the intermolecular Hamiltonian in a body-fixed frame (BF) embedded in the benzene moiety with its origin at the complex's center of mass. We choose this frame to be the same as the $(\hat{x}, \hat{y}, \hat{z})$ axis system defined in

TABLE II. Fixed points of benzene–He intermolecular potential-energy surfaces. The values of the coordinates are in Å and the values of V, measured from the benzene–He dissociation energy, are in cm^{-1}. Fixed points symmetrically equivalent to those listed have been omitted from the table.

	Minima		Saddle points	
	(x,y,z)	V	(x,y,z)	V
IPS-A	(0,0,3.157)	−89.59	(0,5.391,0)	−20.76
	(4.741,0,0)	−44.73	(2.926,0,3.237)	−28.87
IPS-B	(0,0,3.149)	−100.33	(0,5.497,0)	−23.09
			(4.937,0,0)	−40.24
IPS-C	(0,0,3.282)	−66.09	(0,5.462,0)	−17.10
	(2.847,0,2.690)	−43.56	(4.890,0,0)	−28.37
			(1.936,0,3.521)	−35.55
			(0,2.924,3.002)	−31.74
			(0,2.353,3.457)	−30.03

TABLE IV. Calculated intermolecular vibrational energies (in cm^{-1}) of benzene–He for IPS-A.

States	h_6	d_6
$1\,A_1'/1\,A_1''$	0[a]	0[b]
$1\,E_1'/1\,E_1''$	15.75/15.97	16.03/16.14
$2\,A_1'/2\,A_1''$	16.26/16.90	16.82/17.38
$1\,E_2'/1\,E_2''$	17.45/19.72	17.88/20.04
$2\,E_1'/2\,E_1''$	17.47/19.90	17.73/20.02
$1\,B_2'/1\,B_2''$	17.51/20.89	17.90/21.05
$3\,A_1'/3\,A_1''$	18.67/21.00	18.92/21.10

[a]The zero point for the h_6 isotopomer is −29.98 cm^{-1}.
[b]The zero point for the d_6 isotopomer is −30.75 cm^{-1}.

Sec. II B. The intermolecular vibrational Hamiltonian is a function of the position vector, **d**, that points from the benzene center of mass to the He nucleus.[42,43] The components of this vector with respect to the body-fixed axes, expressed as the cylindrical coordinates z, $\rho \equiv \sqrt{x^2+y^2}$, and $\Phi \equiv \tan^{-1}(y/x)$, are the three intermolecular coordinates that we choose for this system. The kinetic-energy portion of the intermolecular vibrational Hamiltonian in these coordinates is given by Eq. (3.15a) of Ref. 44. The specific inertial parameters used here for benzene–He are given in Table III.

The intermolecular Hamiltonian was diagonalized in a symmetry-adapted direct-product basis composed of a one-dimensional harmonic-oscillator discrete variable representation in z (e.g., see Ref. 45) and two-dimensional harmonic-oscillator eigenfunctions in x and y [e.g., see Eqs. (5.1) and (5.2) of Ref. 44]. The relevant molecular symmetry group is $G_{24}=G_{12}\times E^*$, G_{12} being identical to that employed in Ref. 43. (In denoting the irreducible representations (irreps) of G_{24} we use the notation of Ref. 43 and append a single prime for those irreps that are symmetric with respect to E^* and a double prime for those that are antisymmetric.) Values of the parameters defining the primitive basis functions are given in Table III.

Tables IV–VI present results of the $J=0$ calculations for the lowest-energy states of three IPSs. There are several points of note in respect to these results. First, there are significant differences in the zero-point energies of the species (relative to dissociation) for the three IPSs. These differences correlate with the differences in the global-energy minima of the surfaces (see Table II). Second, splittings due to ring–plane crossing are appreciable for many of the levels on all the surfaces, but are particularly prevalent for IPS-A. Indeed,

for that surface all the levels except the zero point are appreciably split. In this regard, it is notable that, of the three surfaces, only IPS-A has minima located in the benzene plane. Third, assignment of most of the states in terms of a doubly degenerate in-plane van der Waals bending mode, ν_β, and a singly degenerate van der Waals stretching mode, ν_σ (such as for benzene–Ar,[28,43,46–51] for example) can be done only nominally, at best. This is because even the lowest energy states involve large-amplitude motions that sample significantly anharmonic regions of the relevant IPS. Having said this, one notes, however, that the $1\,E_1'/1\,E_1''$ states for each IPS have significant ν_β character, as judged by their basis-state compositions. This point is important because it is van der Waals bending fundamentals that have been observed to be the most intense bands in the intermolecular Raman spectra of aromatic–rare gas complexes.[46,50] This leads one to expect strong Raman features at 15.75 cm^{-1} ($1\,E_1' \leftarrow 1\,A_1'$) and 15.97 cm^{-1} ($1\,E_1'' \leftarrow 1\,A_1''$) for IPS-A, at 13.06 cm^{-1} for IPS-B, and at 7.32/7.33 cm^{-1} for IPS-C. We shall examine this expectation more quantitatively below.

C. Rotational constants and Raman intensities

Results from experiment pertaining to the ground-state manifold of benzene–He consist of rotational constants for the zero-point level[5] and intermolecular Raman spectra as reported in Sec. V below. In order to make a connection between these results and possible IPS functions, we have performed calculations of rotational constants and Raman scattering coefficients for the three IPSs. The calculations are based on the results of Ref. 38, wherein it was shown that such molecular constants could be extracted from $J=0$ eigenstates by suitable transformation to an Eckart body-fixed frame.

TABLE III. Basis-set and inertial parameters for intermolecular-state calculations on benzene–He.

$N_z=80$	$\gamma_z=1.40$ Å^{-1}	$z_0=0.0$ Å
$N_\rho=30$	$\gamma_\rho=1.701$ Å^{-1}	$v_{max}=50$
$N_\Phi=102$	$l_{max}=50$	
$m_{He}=4.0026$ amu	$m_{benzene}=78.046\,95$ (84.084)[a] amu	
$I_\perp^b=88.7846$ (107.398) amu-Å^2	$I_\parallel=177.569$ (214.796) amu-Å^2	

[a]Values in parentheses refer to perdeuterated benzene.
[b]$I_\perp$ is the in-plane moment of inertia of benzene and $I_\parallel$ is the out-of-plane moment of inertia of the molecule.

TABLE V. Calculated intermolecular vibrational energies (in cm^{-1}) of benzene–He for IPS-B.

States	h_6	d_6
$1\,A_1'/1\,A_1''$	0[a]	0[b]
$1\,E_1'/1\,E_1''$	13.06[c]	12.78[c]
$2\,A_1'/2\,A_1''$	19.82	19.55
$1\,E_2'/1\,E_2''$	22.82	22.35
$2\,E_1'/2\,E_1''$	27.35/27.36	26.91
$1\,B_2'/1\,B_2''$	29.44/29.46	28.89/28.90
$3\,A_1'/3\,A_1''$	32.08/32.14	31.68/31.72
$1\,B_1'/1\,B_1''$	32.15	31.41
$2\,E_2'/2\,E_2''$	33.72/33.83	33.18/33.23

[a]The zero point for the h_6 isotopomer is -52.57 cm^{-1}.
[b]The zero point for the d_6 isotopomer is -53.09 cm^{-1}.
[c]A single number in a column indicates that the splitting due to ring–plane crossing is less than 0.01 cm^{-1}.

One complication in applying the "Eckart" procedures of Ref. 38 to benzene–He arises because of the ring–plane crossings that are feasible in the species. These very-large-amplitude motions preclude any ready identification of the reference geometry that is necessary for the definition of an Eckart frame.[52,53] We have skirted this complication by working with "single-sided" (G_{12} molecular symmetry group) $J=0$ eigenstates rather than the double-sided ones of Sec. III B. Justification for the validity of this approximation lies in the fact that none of the computed G_{24} zero-point levels of Sec. III B is appreciably split by ring–plane crossing. Consequently, the rotational constants of a G_{24} zero-point state on a given IPS should be the same as the constants corresponding to the G_{12} zero point on the same surface. Similarly, Raman "doorway" states associated with the $G_{24}\,0^{\pm}$ levels should be well-approximated by symmetric and antisymmetric combinations (with respect to E^*) of the relevant doorway state associated with the G_{12} zero point. From these doorway states and the other G_{24} eigenfunctions, polarizability matrix elements (and from them Raman scattering coefficients) involving 0^+ and 0^- as initial states can be computed.

G_{12} eigenstates were computed by the same procedures as employed by us previously for the calculation of $J=0$ intermolecular states of benzene–Ar.[38] The inertial and IPS parameters used were identical to those of the G_{24} calculations described in Sec. III B. As expected from the lack of G_{24} splittings, the computed G_{12} zero-point energies for each isotopomer and for each IPS were identical (to within <0.01

TABLE VI. Calculated intermolecular vibrational energies (in cm^{-1}) of benzene–He for IPS-C.

States	h_6	d_6
$1\,A_1'/1\,A_1''$	0[a]	0[b]
$1\,E_1'/1\,E_1''$	7.32/7.33	7.41[c]
$2\,A_1'/2\,A_1''$	8.92/8.95	8.87/8.90
$1\,E_2'/1\,E_2''$	11.07/11.14	11.00/11.04

[a]The zero point for the h_6 isotopomer is -18.78 cm^{-1}.
[b]The zero point for the d_6 isotopomer is -19.24 cm^{-1}.
[c]A single number in a column indicates that the splitting due to ring–plane crossing is less than 0.01 cm^{-1}.

TABLE VII. Calculated rotational constants (in cm^{-1}) of benzene–helium zero-point levels.

IPS	$\langle|z|\rangle$[a]	B	C
A	3.607	0.1204	0.0956
B	3.428	0.1241	0.0957
C	3.890	0.1120	0.0965
Expt[b]		0.122 ± 0.021	0.098 ± 0.006

[a]The expectation value of z in Å for the state. The same value was used to define the reference geometry for the relevant IPS.
[b]From Ref. 5.

cm^{-1}) to the analogous G_{24} energies. The Eckart reference geometry chosen for a given IPS was that for which the helium lies along the benzene C_6 axis at a distance from the benzene plane equal to the expectation value of z for the relevant zero-point level.

Table VII presents the results of the rotational-constant calculations for the h_6 isotopomers for each of the three IPSs. Also given in the table are experimental results derived from spectroscopy on the $S_1\leftarrow S_0\,6_0^1$ band of benzene–He. Within the rather broad error limits quoted for the experimental results there is agreement with the constants computed for all three surfaces, though those for IPS-A and IPS-B agree best with experiment. In making these comparisons it is important to point out that two, significantly different sets of rotational constants derived from experiment are quoted in Ref. 5. One set was obtained by fitting experimental results after fixing (a) the C constants for the 0_0 and 6^1 levels of the complex to the corresponding A constants in benzene and (b) the Coriolis constant for the 6^1 level of the complex (ζ') to its value in benzene. A second set was obtained by fitting after fixing only ζ'. Herein, we compare our computed results only with the latter set, since the fixing of the C constants to benzene values is unjustified for a species as floppy as benzene–He.

To calculate Raman scattering coefficients we make the assumption that intermolecular Raman bands gain their intensity via the "libration-induced mechanism,"[29,46,50,54,55] wherein cluster polarizability components are modulated during the course of an intermolecular vibration by virtue of the changing projection of the permanent polarizability components of monomer moieties along cluster-fixed axes. With this approximation and Eq. (5.4) of Ref. 38, Raman scattering coefficients were computed from G_{24} doorway states derived from G_{12} zero-point eigenfunctions (see above). In these calculations benzene's polarizability components were taken to be the same as those used in Ref. 50. Table VIII presents calculated scattering coefficients for transitions originating in the $1\,A_1'$ and $1\,A_1''$ (i.e., $0^{\pm}$) levels. The important result is that the $(1\,E_1',1\,E_1'')\leftarrow 0^{\pm}$ transitions are the most intense by a significant amount. Indeed, for IPS-B and IPS-C, no other bands have scattering coefficients within an order of magnitude of these. The results for IPS-A indicate that bands at slightly higher frequencies than the $(1\,E_1',1\,E_1'')\leftarrow 0^{\pm}$ bands might also be observable. One notes, however, that the two $(1\,E_1',1\,E_1'')\leftarrow 0^{\pm}$ bands occur very close to the same frequency, whereas the other bands with appreciable computed scattering coefficients do not

TABLE VIII. Calculated scattering coefficients for intermolecular Raman transitions originating in the zero-point levels of benzene–helium.

	Final state	Transition frequency/cm^{-1}	$S_{v'v}/\text{Å}^6$
IPS-A	$1\,E_1'$	15.75(16.03)[a]	0.64
	$1\,E_1''$	15.97(16.14)	0.84
	$2\,E_1'$	17.47(17.73)	0.32
	$2\,E_1''$	19.90(20.02)	0.21
IPS-B	$1\,E_1'$	13.06	1.66
	$1\,E_1''$	13.06	1.66
	$2\,A_1'$	19.80	0.05
	$2\,A_1''$	19.80	0.05
	$2\,E_1'$	27.34	0.03
	$2\,E_1''$	27.35	0.03
IPS-C	$1\,E_1'$	7.32	2.33
	$1\,E_1''$	7.33	2.34
	$2\,A_1'$	8.91	0.17
	$2\,A_1''$	8.95	0.17

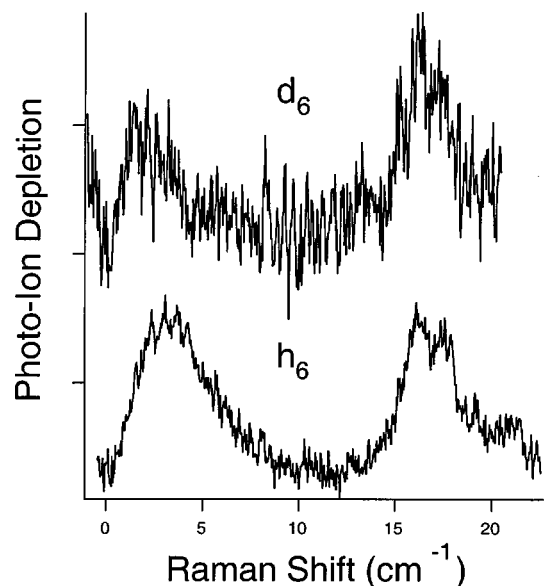[a]Frequencies in parentheses correspond to the perdeuterated isotopomer.

FIG. 2. ILSRS spectra of perdeuterated (top) and perprotonated (bottom) benzene–He. In both cases the parent ion of the pertinent complex was detected.

overlap one another. The point is that, for IPS-A, the overlapped $(1\,E_1',1\,E_1'')\leftarrow 0^{\pm}$ bands are computed to have about five times the intensity of the second-most intense feature in the intermolecular Raman spectrum.

IV. EXPERIMENTAL METHODS

Mass-selective, ionization-loss stimulated Raman spectroscopy (ILSRS) was implemented with an apparatus that has been described elsewhere.[50,54] Briefly, stimulated Raman transitions were driven by a two-color pulse derived from the frequency-doubled output of an injection-seeded Nd:YAG laser and the output of a dye laser pumped by that Nd:YAG laser. The Raman transitions were probed by mass-selective, resonantly enhanced two-photon ionization (R2PI) driven by the frequency-doubled output of a second dye laser. This dye laser was pumped by a second Nd:YAG laser fired at a delay to the first. The R2PI field was tuned so as to yield a photoion signal sensitive to the population of the initial vibrational level involved in the Raman transition. Raman transitions thus registered as depletions in the baseline, mass-selected photoion signal as the Raman frequency was scanned. For this work the stimulated Raman resolution was 0.03 cm^{-1} and the R2PI resolution was about 0.3 cm^{-1}. For a given isotopomer the R2PI field was tuned to the $S_1 \rightarrow S_0\,6_0^1$ band of the species (about 2 cm^{-1} to the blue of the bare benzene 6_0^1 band).[5]

Helium complexes of benzene were formed by passing He gas (at 70 bar) over neat benzene held at 0 °C and then expanding the gas mixture into vacuum through the 0.8-mm diameter orifice of a pulsed valve (General Valve Series 9). The resulting supersonic molecular beam containing the complexes was skimmed before it entered the ion-acceleration region of a time-of-flight mass spectrometer (TOFMS), where it intersected the focused stimulated-Raman and R2PI fields. Photoions were detected at the end of the TOFMS by a dual microchannel plate, the output of which was amplified and directed to a fast oscilloscope and a boxcar integrator. The gate of the boxcar integrator was set so as to average the photoion mass signal arising from the parent ion of the complex being studied. The output of the boxcar was dumped to a computer in synchrony with the scanning of the dye laser used to generate one of the stimulated-Raman fields. In this way the computer collected a spectrum of mass-selected photoions versus stimulated-Raman frequency.

V. EXPERIMENTAL RESULTS

Figure 2 shows intermolecular ILSRS spectra measured for the perprotonated and perdeuterated benzene–^{4}He complexes. In addition to the rotational-Raman features peaked near 4 cm^{-1}, one sees broad structure for both species centered near 16.5 cm^{-1}. Spectra obtained for Raman shifts up to 50 cm^{-1} revealed no other significantly intense, distinct bands.

Figures 3(a)—bottom and 3(b)—bottom show ILSRS band contours in the 13–22 cm^{-1} region of perprotonated benzene–He measured, respectively, for parallel- and perpendicularly polarized Raman fields. These spectra, by the lack of any sharp, polarization-dependent feature, clearly show that the Raman structure arises from an anisotropic Raman band(s). In this respect the data are consistent with the intensity being due, at least in part, to the $(1\,E_1',1\,E_1'')\leftarrow 0^{\pm}$ bands computed (for all three IPSs) to be the dominant features in the intermolecular Raman spectra. We have explored this point further by comparing the observed contours with simulated $(1\,E_1',1\,E_1'')\leftarrow 0^{\pm}$ band contours. In the simulations we have taken account of the fact that one of the linearly polarized stimulated-Raman fields is intense enough to produce optical-field-induced pendular states when interacting with the anisotropic polarizability of the benzene–He complex. In other words, we have simulated *pendular* band contours. A description of the procedure employed for these simulations is given in Ref. 50. The values of the parameters used in the calculations are as follows: The rotational con-
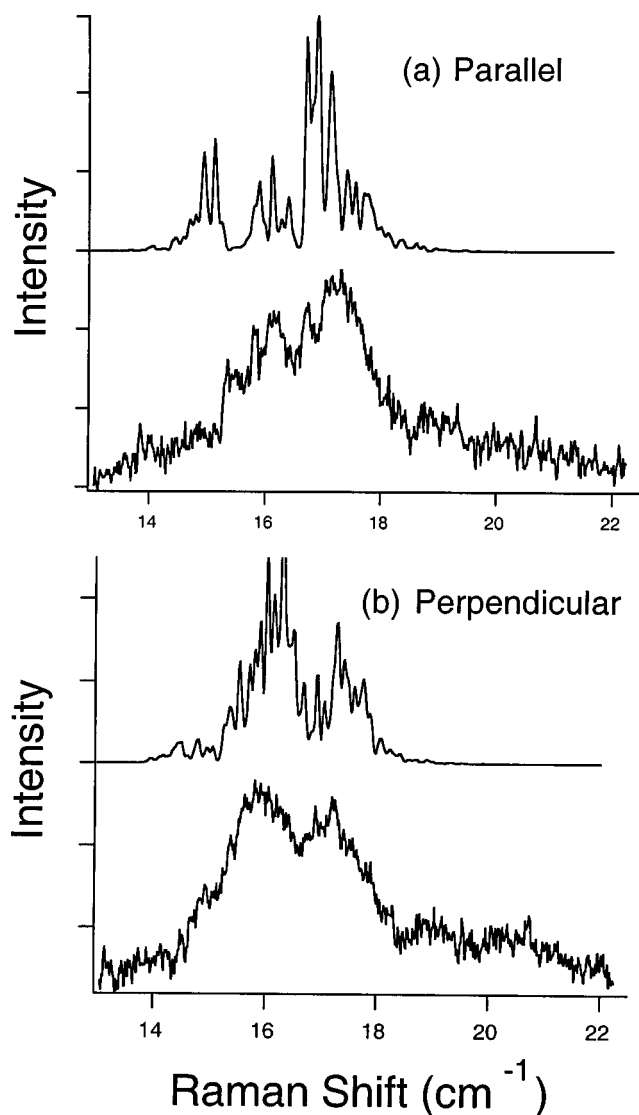
FIG. 3. Stimulated-Raman band contours of perprotonated benzene–He taken with the two stimulated Raman fields polarized (a) parallel and (b) perpendicular to one another. In both (a) and (b) the bottom trace is a measured ILSRS spectrum and the top trace is a pendular band contour calculated according to details provided in the text.

stants for the $0^{\pm}$ states were taken to be those given in Table VII for IPS-A. Those for $1\,E_1'$ and $1\,E_1''$ were taken as $B = 0.1087\,\mathrm{cm}^{-1}$, $C = 0.1003\,\mathrm{cm}^{-1}$, and $2C\zeta = 0.1194\,\mathrm{cm}^{-1}$ (ζ being the first-order Coriolis constant). These were computed from the $G_{12}\,1E_1\,J=0$ eigenstate for IPS-A as per the procedure described in Sec. III C. The polarizability anisotropy of the complex was assumed to be $\alpha_{\|} - \alpha_{\perp} = -6.6\,\text{Å}^3$.[56] The optical-field intensity was taken as $2\times10^{10}\,\mathrm{W\,cm}^{-2}$, and the sample temperature was assumed to be 1 K (both values approximate experimental conditions). The top traces in Figs. 3(a) and 3(b) show pendular band contours computed for parallel- and perpendicularly polarized Raman fields, respectively. While quantitative matches between these calculated contours and the corresponding measured ones of Fig. 3 cannot be expected owing to (i) the spatial and temporal variation of the experimental optical-field intensity; (ii) the likely overlap of *two* bands in the measured spectra; and (iii) uncertainties in the molecular constants and experi-

mental parameters, one sees clearly that there is good qualitative agreement in regard to the overall shapes and widths of the contours. This agreement solidifies the assignment of the dominant structure as the pendular bands of the $(1\,E_1',1\,E_1'')\leftarrow0^{\pm}$ transitions. Further, it allows for an estimate of 16.0 cm^{-1} as the average of the band centers of these transitions. Finally, the comparison between computed and measured band contours strongly suggests that the weak structure in the 18–22 cm^{-1} region of the measured spectra is due to bands other than the $(1\,E_1',1\,E_1'')\leftarrow0^{\pm}$ ones.

With the foregoing, one is in a position to assess the degree to which the experimental Raman results match the results of the computations based on each of the three IPSs (Table VIII). One concludes that the experimental results match very well those computed under the assumption that *IPS-A governs the benzene–He interaction*. Both the h_6 and the d_6 species have a dominant intermolecular Raman feature near 16.0 cm^{-1}, just where the IPS-A calculations predict that the $(1\,E_1',1\,E_1'')\leftarrow0^{\pm}$ bands should occur with five times more (integrated) intensity than any other intermolecular band. Further, the weaker structure at 18–22 cm^{-1} in the experimental data matches the expectation, based on IPS-A calculations, that the $(2\,E_1',2\,E_1'')\leftarrow0^{\pm}$ Raman bands should appear in just this spectral region with sufficient intensity to be observable. Compared with the IPS-A results, however, the calculated results based on both IPS-B and IPS-C are in significantly worse agreement with experiment. Both sets of calculations predict too-small frequencies for the $(1\,E_1',1\,E_1'')\leftarrow0^{\pm}$ main bands. Both also lead to the expectation that these main bands will likely be the only ones with observable intensity in the spectra. The upshot is that IPS-A gives a much more accurate accounting of the experimental Raman observables of benzene–He than either of the other two surfaces.

It is pertinent to consider reasons as to why the two literature IPSs considered in this work are significantly less accurate than IPS-A in respect to their agreement with measured intermolecular Raman spectra. IPS-B is of the atom–atom Lennard-Jones form. While such a form has the virtues of simplicity and ease of calculation, the absence of multiatom terms renders it deficient in the quantitative modeling of aromatic–atom IPSs.[26,47,48,57] One particular manifestation of this deficiency is the significant underestimation of intermolecular bending frequencies.[58] Such underestimation in the case of benzene–He may be expected to lead to too-small frequencies for the $(1\,E_1',1\,E_1'')\leftarrow0^{\pm}$ transitions (as observed), since these transitions have significant bending-fundamental character. IPS-C is also a pairwise-additive, atom–atom potential and lacks three-body and higher terms. Moreover, its parameters are derived[24] from a fit to *ab initio* data computed[37] at a lower level than that reported here. Hence, the significant deviation of the calculated IPS-C Raman results from experimental results is also not unexpected.

VI. CONCLUSION

Analytic IPS functions obtained by fitting to CCSD(T) *ab initio* results have yielded good agreement with experiment for the benzene–Ar (Ref. 27) and benzene–N$_2$ (Ref.

29) complexes. In both cases rotational-constant and intermolecular-level-structure data from experiment have been reproduced in calculations employing such IPSs. In the present report, we have shown that a similar situation applies to benzene–He. While the experimental data on benzene–He are not as extensive as for these other complexes, those that do exist are completely consistent with the fitted IPS reported herein (IPS-A). Benzene–He thus serves as a further example of the utility of CCSD(T) calculations in mapping out accurate IPSs for weakly bound complexes.

ACKNOWLEDGMENTS

[1] R. E. Smalley, D. H. Levy, and L. Wharton, J. Chem. Phys. **64**, 3266 (1976).
[2] R. E. Smalley, L. Wharton, and D. H. Levy, J. Chem. Phys. **68**, 671 (1978).
[3] R. E. Smalley, L. Wharton, D. H. Levy, and D. W. Chandler, J. Chem. Phys. **68**, 2487 (1978).
[4] W. Sharfin, K. E. Johnson, L. Wharton, and D. H. Levy, J. Chem. Phys. **71**, 1292 (1979).
[5] S. M. Beck, M. G. Liverman, D. L. Monts, and R. E. Smalley, J. Chem. Phys. **70**, 232 (1979).
[6] J. E. Kenny, K. E. Johnson, W. Sharfin, and D. H. Levy, J. Chem. Phys. **72**, 1109 (1980).
[7] D. H. Levy, C. A. Haynam, and D. V. Brumbaugh, Faraday Discuss. **73**, 137 (1982).
[8] T. S. Zwier, E. Carrasquillo, and D. H. Levy, J. Chem. Phys. **78**, 5493 (1983).
[9] C. A. Haynam, D. V. Brumbaugh, and D. H. Levy, J. Chem. Phys. **80**, 2256 (1984).
[10] E. R. Bernstein, K. Law, and M. Schauer, J. Chem. Phys. **80**, 634 (1984).
[11] C. A. Taatjes, W. B. Bosma, and T. S. Zwier, Chem. Phys. Lett. **128**, 127 (1986).
[12] K. Yamanouchi, S. Isogai, and S. T. Kuchitsu, Chem. Phys. **116**, 123 (1987).
[13] D. O. DeHaan, A. L. Holton, and T. S. Zwier, J. Chem. Phys. **90**, 3952 (1989).
[14] T. S. Zwier, J. Chem. Phys. **90**, 3967 (1989).
[15] D. H. Semmes, J. S. Baskin, and A. H. Zewail, J. Chem. Phys. **92**, 3359 (1990).
[16] B. Coutant and P. Bréchignac, J. Chem. Phys. **100**, 7087 (1994).
[17] A. Bach, S. Leutwyler, D. Sabo, and Z. Bačić, J. Chem. Phys. **107**, 8781 (1997).
[18] J. Williams, A. Rohrbacher, J. Seong *et al.*, J. Chem. Phys. **111**, 997 (1999).
[19] U. Even, J. Jortner, D. Noy, N. Lavie, and C. Cossart-Magos, J. Chem. Phys. **112**, 8068 (2000).
[20] I. Al-Hroub, U. Even, and J. Jortner, J. Chem. Phys. **115**, 2069 (2001).
[21] A. Heidenreich, U. Even, and J. Jortner, J. Chem. Phys. **115**, 10175 (2001); A. Heidenreich and J. Jortner, *ibid.* **118**, 10101 (2003).
[22] For example, see the thematic issues of Chem. Phys. **239**, 1 (1998) Chem. Rev. **100**, 3861 (2000), and references therein.
[23] M. Hartmann, A. Lindinger, J. P. Toennies, and A. F. Vilesov, Chem. Phys. **239**, 139 (1998).
[24] Y. Kwon and K. B. Whaley, J. Chem. Phys. **114**, 3163 (2000).
[25] K. Raghavachari, G. W. Trucks, J. A. Pople, and M. Head-Gordon, Chem. Phys. Lett. **157**, 479 (1989).
[26] H. Koch, B. Fernández, and O. Christiansen, J. Chem. Phys. **108**, 2784 (1998).
[27] H. Koch, B. Fernández, and J. Makarewicz, J. Chem. Phys. **111**, 198 (1999).
[28] B. Fernández, H. Koch, and J. Makarewicz, J. Chem. Phys. **111**, 5922 (1999).
[29] S. Lee, J. Romascan, P. M. Felker, T. B. Pedersen, B. Fernández, and H. Koch, J. Chem. Phys. **118**, 1230 (2003).
[30] S. F. Boys and F. Bernardi, Mol. Phys. **19**, 553 (1970).
[31] T. Helgaker, H. J. Aa. Jensen, P. Jørgensen *et al.*, DALTON, a molecular electronic structure program, Release 1.2, 2001. See http://www.kjemi.uio.no/software/dalton/dalton.html
[32] H. Koch, A. S. de Meras, T. Helgaker, and O. Christiansen, J. Chem. Phys. **104**, 4157 (1996).
[33] H. Koch, P. Jørgensen, and T. Helgaker, J. Chem. Phys. **104**, 9528 (1996).
[34] See EPAPS Document No. E-JCPSA6-119-022348 for the coordinates of the grid points, the values of the *ab initio* interaction energies at the grid points, and the deviations of the fitted IPS from the *ab initio* energies. A direct link to this document may be found in the online article's HTML reference section. The document may also be reached via the EPAPS homepage (http://www.aip.org/pubservs/epaps.html) or from ftp.aip.org in the directory /epaps/. See the EPAPS homepage for more information.
[35] P. R. Bevington, *Data Reduction and Error Analysis for the Physical Sciences* (McGraw-Hill, New York, 1969).
[36] T. B. Pedersen, B. Fernandez, H. Koch, and J. Makarewicz, J. Chem. Phys. **115**, 8431 (2001).
[37] P. Hobza, O. Bludsky, H. L. Selzle, and E. W. Schlag, J. Chem. Phys. **97**, 335 (1992).
[38] P. M. Felker, D. Neuhauser, and W. Kim, J. Chem. Phys. **114**, 1233 (2001).
[39] D. Neuhauser, J. Chem. Phys. **93**, 2611 (1990); **100**, 5076 (1994).
[40] M. R. Wall and D. Neuhauser, J. Chem. Phys. **102**, 8011 (1995).
[41] V. A. Mandelshtam and H. S. Taylor, J. Chem. Phys. **106**, 5085 (1997).
[42] G. Brocks and D. van Koeven, Mol. Phys. **63**, 999 (1988).
[43] For example, A. van der Avoird, J. Chem. Phys. **98**, 5327 (1993).
[44] W. Kim, D. Neuhauser, M. R. Wall, and P. M. Felker, J. Chem. Phys. **110**, 8461 (1999).
[45] M. Mandziuk and Z. Bačić, J. Chem. Phys. **98**, 7165 (1993).
[46] P. M. Maxton, M. W. Schaeffer, S. M. Ohline, W. Kim, V. A. Venturo, and P. M. Felker, J. Chem. Phys. **101**, 8391 (1994).
[47] Th. Brupbacher, J. Makarewicz, and A. Bauder, J. Chem. Phys. **101**, 9736 (1994).
[48] J. Makarewicz and A. Bauder, Mol. Phys. **84**, 853 (1995).
[49] E. Riedle and A. van der Avoird, J. Chem. Phys. **104**, 882 (1996).
[50] W. Kim and P. M. Felker, J. Chem. Phys. **107**, 2193 (1997).
[51] R. Neuhauser, J. Braun, H. J. Neusser, and A. van der Avoird, J. Chem. Phys. **108**, 8408 (1998).
[52] C. Eckart, Phys. Rev. **47**, 552 (1935).
[53] J. D. Louck and H. W. Galbraith, Rev. Mod. Phys. **48**, 69 (1976).
[54] W. Kim, M. W. Schaeffer, S. Lee, J. S. Chung, and P. M. Felker, J. Chem. Phys. **110**, 11264 (1999).
[55] W. Kim, S. Lee, and P. M. Felker, J. Chem. Phys. **112**, 4527 (2000).
[56] This is the polarizability anisotropy of the benzene molecule. For example, see J. O. Hirschfelder, C. F. Curtis, and R. B. Bird, *Molecular Theory of Gases and Liquids* (Wiley, New York, 1954), p. 950.
[57] P. M. Weber, J. T. Buontempo, F. Novak, and S. A. Rice, J. Chem. Phys. **88**, 6082 (1988).
[58] A. R. Tiller and D. C. Clary, J. Chem. Phys. **92**, 5875 (1990).